Pharmacological validation of SSc-ILD mouse model bleomycin-induced by osmotic minipump

Francesca Ravanetti
University of Parma
Erica Ferrini
University of Parma
Luisa Ragionieri
University of Parma
Zahra Khalajzeyqami
University of Bologna
Maria Nicastro
University of Parma
Yanto Ridwan
Erasmus University Rotterdam
Alex Kleinjan
Erasmus University Rotterdam
Gino Villetti
Chiesi (Italy)
Andrea Grandi
Chiesi (Italy)
Franco Fabio Stellari (fb.stellari@chiesi.com)
Chiesi (Italy)

Research Article

Keywords: Osmotic minipump, nintedanib, bleomycin, lung and skin fibrosis, micro-CT

Posted Date: May 7th, 2021

DOI: https://doi.org/10.21203/rs.3.rs-493155/v1

Abstract

Systemic sclerosis (SSc) is an autoimmune disease characterized by an excessive production and accumulation of collagen in the skin and internal organs often associated with interstitial lung disease (ILD).

The unknown pathogenetic mechanisms of SSc-ILD and the lack of animal models mimicking the features of the human disease contribute to create a gap between the selection of antifibrotic drug candidates and effective therapies.

Nintedanib (NINT) was used as a tool compound to validate the pharmacological response either on lung or skin fibrosis in a SSc-ILD mouse model.

The model is based on the continuous infusion of bleomycin (BLM) by osmotic minipumps for 1 week in the C57BL/6 female mice.

Longitudinal Micro-CT analysis highlighted a significant slowdown in lung fibrosis progression after NINT treatment, then confirmed by histology. However, no significant effect was observed on lung hydroxyproline content, inflammatory infiltrate and skin lipoatrophy.

The modest pharmacological effect reported reflects the clinical outcome, lighting up the reliability of this model to serve as secondary screening to profile the best clinical drug candidates. Moreover, we have underlined the pivotal role of Micro-CT imaging, together describing the relevant readouts and the importance of their validation prior to use for drug discovery.

Introduction

Systemic sclerosis (or scleroderma) (SSc) is an autoimmune disease of unknown aetiology, characterized by vasculopathy, excessive fibrous tissue generation and aberrant immune activation resulting in damage to various organs including the skin, esophagus, heart, lungs, and kidneys [1,2]. Most critically, about 80% of SSc patients develop pulmonary dysfunctions such as pulmonary hypertension and associated interstitial lung disease (ILD), this latter characterized by early immune cell infiltration followed by various degree of fibrosis and gas exchange impairment that significantly reduces life expectancy [3–5]. The pronounced uncertainty surrounding the pathogenetic mechanisms behind SSc-ILD and the absence of effective treatments for this disorder have solicited the creation of *ad hoc* animal experimental models capable of mimicking the different clinical and pathological peculiarities of SSc-ILD in humans [6–8].

Bleomycin (BLM) is the commonest agent used to replicate some ILD key hallmarks, such as changes in pulmonary histoarchitecture, fibroblast/myofibroblast activation, and collagen deposition [9–11]. Over the past few years, many studies have tested various methods of BLM administration [12–14].

In a recently published paper, an experimental model of human SSc-ILD in C57BL/6 mice has been described. This model involved a continuous and controlled release of BLM by subcutaneously implanted osmotic mini-pumps [15]. Before using a new animal model in drug discovery, its reproducibility, robustness and ability to respond to pharmacological treatments should be validated. The selection of the best drug candidate to be introduced into the clinic depends on many factors, but a head-to-head comparison with a gold standard therapy has an important role. Several crucial points, such as time, doses of administration and different readouts, are essential to provide the best view on how drugs are performing in animal models, since each model can respond to the same therapy in a different manner.

A model inducing subacute - chronic fibrosis through the release of BLM by osmotic mini-pumps allows evaluation about the effects of antifibrotic compounds, either in the skin or in the lungs, since the target fibrotic lesions have been identified in both organs [15–17].

The main purpose of this study was to examine the antifibrotic activity of nintedanib (NINT), a tyrosine-kinase inhibitor used to treat idiopathic pulmonary fibrosis and recently approved as a therapy for SSc associated with ILD [18,19], in the aforementioned SSc-ILD mouse model.

In the present research, NINT was orally administered for two weeks following a therapeutic protocol, starting at day 14 [20,21]. In order to use this fibrosis model for secondary screening in our pipeline several readouts were considered. The lung fibrosis progression and the pharmacological response to treatment were longitudinally assessed by micro-CT, and then corroborated by histological analyses in lung and skin samples at the endpoint experiment.

Materials And Methods

Animal model

Twenty-four 7-8-week-old C57BL/6 female mice (Envigo, Italy) were kept in a conventional animal facility in ventilated cages with free access to standard rodent chow and softened tap water at least 7 days prior to use. All mice were randomly subdivided into two groups: 8 were treated with saline and 16 with BLM.

Ethical statement

All experiments were carried out in the animal unit of Chiesi Farmaceutici, an AAALAC International-accredited facility, in accordance with the intramural animal-welfare practices for animal experimentation approved by the Animal Welfare Body of Chiesi Farmaceutici and authorized by Italian Ministry of Health (protocol number: 449/2016-PR). The study was also in compliance with the European Directive 2010/ 63 UE, Italian D.Lgs 26/2014 as well as the revised “Guide for the Care and Use of Laboratory Animals” released by the National Research Council Committee (US, 2011) [22] and reported in accordance with ARRIVE guidelines [23].

Experimental design

Each mouse was anesthetized with 2.5% isoflurane mixed with oxygen, the implantation site was shaved and, through a small incision, a subcutaneous pocket was created on the left-hand side of its back using the jaws of a hemostat clamp. The osmotic minipumps [ALZET 1007D; DURECT, (release rate 0.5 µl/h for 7 days), Cupertino, CA] containing either 100 µl saline or BLM (Baxter Oncology GmbH, 60mg/kg dissolved in saline) were implanted and removed after 8 days. At day 14, BLM mice were randomly divided in two groups, receiving either NINT (Carbosynth, 60mg/kg/die) dissolved in Tween80 0.05% in saline or vehicle (Tween80 0.05% in saline), by gavage, daily for two weeks (**Fig. 1**).

The animals were monitored and weighed daily throughout the experimental procedure.

A Visual Analogue Scale (0-10) for pain assessment was assessed daily by a designed veterinarian or trained technicians. VAS ≥7 and/or body weight loss ≥ 20% were considered as humane endpoints, as well as signs of dyspnoea or apathy evaluated by a designed veterinarian.

Micro-computed tomography acquisition protocol

Micro-computed tomography (micro-CT) lung imaging was performed longitudinally at day 14 and 28 by Quantum GX Micro-CT (PerkinElmer, Inc. Waltham, MA). Each mouse was anesthetized using 2% isoflurane and then positioned inside the CT scan. Images were acquired with the following parameters: X-ray tube voltage 90 KV, X-ray tube current 88 µA and total scan time of 4 minutes. A ring reduction correction was applied to the sinograms and the entire set of projection radiographs was entered into a GPU-based filtered back-projection algorithm with a Ram-Lak filter [24]. The acquisition protocol in 'high resolution' mode resulted in one 3D dataset with 50 µm isotropic reconstructed voxel size.

Image post-processing: lung segmentation protocols and analysis.

For each acquisition, a stack of 512 cross-sectional images was produced. The reconstructed datasets were analyzed using the Perkin Elmer Analyze software (Analyze 12.0; Copyright 1986-2017, Biomedical Imaging Resource, Mayo Clinic, Rochester, MN). The images stacks were filtered and converted from grey levels to CT numbers (Hounsfield Units - HU). The conversion is a linear transformation setting -1000 HU as the density of air and 0 HU as the density of water. A semi-automatic segmentation was used to extract airways and lungs. For the quantitative assessment of the lung parenchyma, HU clinical ranges were applied on rescaled HU images to the segmented lung volume to define normo-aerated [(-900, -500) HU] and poorly-aerated [(-500, -100) HU] tissues [25]. The two compartments with a different aeration degree were expressed as percentage of the total lung volume. The poorly-aerated tissue refers to a low gas/tissue ratio and it was used to quantify lung fibrosis progression and evaluate the efficacy of NINT [26].

Bronchoalveolar lavage, cytokines, and matrix metalloproteinases.

After micro-CT imaging at day 28, all mice were euthanized with an overdose of anesthetic follow by bleeding from the abdominal aorta. Bronchoalveolar lavage fluid (BALF) was collected by gently washing

the bronchial tree using 0.6 mL sterile solution three times [Hank's balanced salt solution (HBSS) ×10; ethylenediaminetetraacetic acid (EDTA) 100 mM; 4-(2-hydroxy-ethyl)-1-piperazineethansulphonic acid (HEPES) 1 mM; distilled water]. The samples were centrifuged at 300 x g for 10 minutes at 4°C and the supernatant collected and frozen for further investigation. The cellular pellet was resuspended in 0.2 mL of BALF solution and total white blood cells (WBC) were measured using an automated cell counter (Dasit XT 1800J). Afterwards, about $1.0x10^6$ cells were also used to quantify the M2 macrophage population by flow cytometry. The cells were suspended in FACS Buffer (PBS; 0.5% BSA) and in the lysis buffer to remove red blood cells (BD Bioscience). Then the cells were stained with anti-CD206 (Bio-Rad), anti-F4/80 (BioLegend) and anti-CD11b (BioLegend) antibodies, washed, and finally acquired using a FACS Canto II Cytometer (BD Bioscience) and analyzed with FACS Diva software. The total macrophage population was selected based on forward (FSC) versus side scatter (SSC) plots, and, subsequently, M2 macrophages were identified in terms of total number of anti-$CD206^+$ events within a F4/80-CD11b positive selected population.

The matrix metalloproteinases 2 and 9 (MMP-2 and MMP-9, respectively) and metallopeptidase inhibitor 1 (TIMP-1) concentrations in BALF were assessed by enzyme-linked immunosorbent assay (ELISA) kit (R&D Systems, Minneapolis, USA). The protein concentrations were measured by interpolation from the standard curve and were expressed in fold of increase (FOI).

Histological analysis and fibrosis quantification

The whole left lung and skin from the left gluteal region (*i.e.,* distant from the implant site to avoid dermal fibrosis artifact) were excised. The skin and the lung were fixed with 10% paraformaldehyde and embedded in paraffin. Serial 5 µm thick sagittal sections were stained with hematoxylin-eosin (H&E) to demonstrate the general tissue morphology, and with Masson's trichrome (MT) to evaluate the collagen-based matrix. Whole slide images (WSI) were acquired using NanoZoomer S60 scanner (Hamamatsu Photonics, K.K., Japan). Two independent researchers with experience in animal models of lung fibrosis performed blind histological analyses.

The extent of fibrosis was morphologically and qualitatively assessed in a subpleural frame (Region of Interest) of lung parenchyma (250 µm thickness, **Fig. 2(a)**). The fibroproliferative modifications in the frame area were evaluated through the semiquantitative 0-to-8 Ashcroft score. The Ashcroft frame scores were subsequently categorized into mild (mean score from 0 to 3), moderate (4) and severe (5-8). Moreover, the fibrotic foci within the frame were quantified based on morphological and colorimetric thresholds and labelled as "areas of interest" (AOI). The extent of fibrosis was evaluated through the following histomorphometric parameters: 1) mean number of fibrotic foci per mm^2 of parenchyma; 2) focus size (small, if its area was <7,500 mm^2; large, if >7,500 mm^2); 3) fraction of Frame occupied by total AOI area (SAOI area/Frame surface), as a percentage value.

For the skin samples, the histomorphometric parameters considered in the MT stained sections were: 1) dermis thickness, defined as the mean distance between the epidermal-dermal junction and the dermal-

subcutaneous junction [16]; 2) hypodermis thickness, defined as the mean distance between the dermal-subcutaneous junction and the muscle layer. The inflammatory infiltrate was evaluated on sections stained with H&E by a semiquantitative method using a 0 to 4 grade score, reflecting increasing inflammation, as described by Gallet et al. (2011) [27]. Measurements were carried out in five randomly selected fields from one sample from each animal.

Collagen content

The collagen-based extracellular matrix was measured using the image analysis software NIS-Elements AR 3.1 (Nikon Tokyo) in the TM-stained lung sections after selection of a correct green threshold detected on the Light Green stained collagen fibers to eliminate air spaces and bronchial epithelium [28].

Hydroxyproline quantification

The right lung lobes were used to quantify the collagen indirectly through hydroxyproline (Hyp) concentration using a commercial kit (Sigma Aldrich) in accordance with the manufacturer's protocol. In brief, the lobes were homogenized in PBS, hydrolyzed in 6 N HCl for 24 hours at 100°C and finally neutralized in 6N NaOH. The final Hyp concentration was determined by the reaction of oxidized Hyp with 4-Dimethylamino benzaldehyde (DMAB), which resulted in a colorimetric product, proportional to the Hyp content. This reaction was measured at a wavelength of 560 nm and, finally, each total amount of Hyp was normalized for the relevant right lobe weight.

Immunofluorescence staining

Immunofluorescent (IF) reactions to detect M2-like polarized macrophages were performed on paraffin embedded sections (16). Briefly, sections were incubated using an anti-CD206 primary antibody (1 µg/mL, AF2535; R&D Systems). This reaction was revealed by a secondary donkey anti-goat antibody Alexa Fluor 488 conjugate (3 µg/mL, AB2336933; Jackson Laboratories). Lastly, the nuclei were counterstained with DAPI (Invitrogen). For negative control the primary antibody was omitted and tissues were incubated in 10 mM phosphate buffer or, alternatively, with unlabelled rabbit IgG nonimmune isotype control (2009-1; Alpha Diagnostic International) used at the same concentration as the selective antibody. Fluorescent WSI were acquired using NanoZoomer S60 (Hamamatsu Photonics, K.K.).

Statistical analysis

Statistical analysis was performed using one-way ANOVA followed by Dunnett's *t* test, to compare each group with the BLM group as control. For micro-CT data a two-way ANOVA test was performed to compare each group with the BLM group and to compare different time points of observation, using Dunnett's and Sidak's tests for multiple comparisons, respectively. The comparison of the frequency distribution was performed with a Chi-squared test. Statistics were carried out using GraphPad Prism 7.0 software (GraphPad; La Jolla, CA, USA). Sample size was calculated with A-priori Power Analysis

(G*Power Version 3.1.2) considering Ashcroft Score as endpoint. A value of $P<0.05$ was considered statistically significant. Data are expressed as means and S.E.M.

Results

Experimental Animals

BLM induced a weight loss up to a maximum reduction of 18% at day 14 but, as expected, mice recovered at later time points.

NINT showed a well-tolerated profile, since no difference in body weight was identified compared to the BLM group. The Saline group did not exhibit any distress and no weight loss was observed (**Supplementary Fig. 1**).

Morphology and fibrosis quantification in subpleural tissue

MT staining highlighted different morphological features in the lungs of BLM and BLM+NINT groups, as compared to the normal parenchyma of the Saline group. The fibrotic lesions were mainly located in the subpleural lung parenchyma (frame, **Fig. 2(a)**) in both BLM and BLM+NINT groups and were characterized by collagen deposition with thickening alveolar septa and moderate inflammatory infiltrate.

Representative foci histological features and conglomerations are presented in **Fig. 2(b-d)**.

BLM induced a significant increase in Ashcroft score compared to Saline, while NINT treatment significantly inhibited lung fibrosis (21%) (**Fig. 2(e)**).

The frequency distribution of Ashcroft score values showed predominantly mild (85%) and moderate (14%) lesions in BLM group. The antifibrotic treatment modulated the fibrosis, increasing the percentage of mild (94%) and decreasing the moderate (6%) fibrotic lesions (**Fig. 2(f)**).

In accordance with the Ashcroft score, collagen content percentage was significantly reduced in NINT-treated mice compared to the BLM group (18%) (**Fig. 2(g)**).

The effect of NINT was also investigated for number of foci/mm^2 and SAOI area/Frame (%). This analysis highlighted significant differences between the Saline and BLM groups, but was not able to discriminate the efficacy of the antifibrotic therapy, since both these parameters were not significantly reduced by the NINT treatment (**Fig. 2(h-j)**). Similarly, the quantification of Hyp in the lungs of the BLM group was significantly higher compared to Saline but not significantly reduced by NINT treatment (**Fig. 2(i)**).

BLM induced pulmonary inflammation by recruiting white blood cells (WBC), (**Supplementary Fig. 2(a)**). NINT treatment significantly reduced (40%) the total number of WBC measured in BALF, but only a modest inhibition was observed on the macrophage (26%), lymphocyte (24%) and neutrophil (33%)

populations (**Supplementary Fig. 2(b-d)**). We have investigated the effect of NINT on the M2-like macrophages cell population in BALF, using a flow cytometry technique with CD206 as a surface marker. FACS analysis revealed a marked increase in M2-like cells in BLM-treated mice, compared to Saline, however no significant level of inhibition was observed in the BLM+NINT group (**Fig. 3(g)**).

IF staining of lung tissue after bronchoalveolar lavage confirmed the presence of residual M2-like macrophages in both BLM and BLM+NINT-treated mice (**Fig. 3(a-f)**).

Antifibrotic treatment decreased MMP-2 (40%), MMP-9 (50%) and TIMP-1 (28%) concentrations in BALF, however, statistical significance was reached only for MMP-9 (**Fig. 4(a-c)**).

Another goal of this study was to evaluate the activity of NINT treatment on skin fibrosis. The most evident changes in skin morphology of BLM and BLM+NINT, compared to Saline, are due to lipoatrophy (**Fig. 5(a-c)**). No significant differences were found in dermis thickness (**Fig. 5(d)**), while a significant decrease in hypodermis thickness was observed in both BLM and BLM+NINT compared to Saline-treated mice (**Fig. 5(e)**). Finally, a moderate pro-inflammatory effect of BLM was revealed in skin and only a slight modulation was induced by NINT treatment (**Fig. 5(f)**).

Micro-CT

Longitudinal micro-CT imaging was performed at 14 (baseline) and 28 days, representing the beginning and the end of NINT treatment.

Representative micro-CT scans of BLM and BLM+NINT-treated mice showed an increase in the poorly-aerated tissue along with a decrease in the normo-aerated tissue (pink and blue, respectively) at 28 days compared to baseline (**Fig. 6(a)**). On the contrary, Saline lungs were largely composed of normally-aerated tissue and remained unchanged over time.

Poorly-aerated lung compartment was used as a marker of fibrosis, thus longitudinally quantified for each group (**Fig. 6(b)**). These data revealed that fibrosis was uniformly distributed at the baseline for BLM and BLM+NINT groups since the percentage of poorly-aerated tissue was not significantly different. The fibrosis progression was detected in both BLM and BLM+NINT groups at day 28; however statistical significance was achieved only for BLM group compared to baseline (**Fig. 6(b)**).

As previously reported, no alteration in Saline lung parenchyma was reported, in fact, the amount of poorly-aerated tissue was constant throughout the experiment (**Fig. 6(b)**).

The quantification of normally and poorly-aerated lung compartments is usually performed at the end of the experiment to evaluate the efficacy of the pharmacological treatment with respect to BLM control group (**Fig. 6(c)**). Although poorly-aerated tissue was higher in both BLM or BLM+NINT-treated animals (70 and 54%) compared to Saline (22%), NINT treatment significantly limited this worsening (-23%) compared to vehicle-treated mice (**Fig. 6(c)**).

Discussion

Despite the great advances in knowledge of the etiopathogenesis of SSc-ILD in recent years, medical need remains very high. In particular, it is imperative to find reproducible and relevant animal models capable of reproducing the chronic and progressive aspects of the disease, and to provide robust readouts in order to test putative new drugs [20,21]. Furthermore, new technologies need to be fully integrated into the antifibrotic drug development process for the screening of the best compounds to advance in clinical therapy.

In this study, we explored the antifibrotic effects of NINT on lung and skin fibrosis in a SSc-ILD mouse model, by using different readouts including micro-CT imaging.

NINT showed a significant inhibition of the total Ashcroft score and collagen deposition.

Although the antifibrotic treatment effect was less pronounced on the Ashcroft frequency distribution, the number of fibrotic foci/mm ^{2} and Σ AOI/frame (%), these parameters may still provide important information either to monitor the inter-experiment reproducibility of fibrosis or to evaluate drug efficacy.

Hyp was not significantly modulated by the NINT treatment. Even though Hyp is commonly considered an important readout, in our drug screening experiments concerning BLM-induced lung fibrosis models, we always observed high variability and poor inter-experiments reproducibility. As previously reported, the fibrotic lesions, mainly localized in the subpleural area, could be underestimated if evaluated over the whole parenchyma [29]. Similarly, the quantification of Hyp could be affected by the size of the sampling site. For this reason, a FOI of 2 between Saline and BLM raises serious questions about whether this range will be sufficient to evaluate any antifibrotic effect in this model.

Hyp determination, being a destructive assay, precludes other histological analyses or alternative readouts that might be considered [30].

A significant anti-inflammatory activity of NINT was noted only on WBC in BALF; on the contrary, only a mild and non-significant inhibition was observed in the M2-like population by FACS. Although the pivotal role of macrophages in IPF has been recently well reported [31,32], the modulatory effect of NINT on macrophage polarization *in vivo* has been only demonstrated in Fra2 transgenic mice, ameliorating histological features of pulmonary arterial hypertension [33]. In human macrophages, NINT treatment was able to downregulate M2 markers of expression *in vitro* [34]. Although NINT showed a modest inhibitory effect in our mouse model, we found that M2-like cells may represent a useful readout for evaluating the antifibrotic drug effect, since it might be directly linked to fibrosis.

NINT modulated levels of matrix metalloproteinases in BALF samples compared to vehicles, however achieving statistical significance only for MMP-9. This could be explained by the fact that MMP-9 is mainly expressed by inflammatory cells, whereas MMP-2 is especially released by epithelial cells [35].

Their tissue inhibitor, TIMP-1, is expressed by the interstitial cells in the fibrotic areas during wound healing [35]. TIMP-1 levels remain high in the BALF up to day 21 [29], corresponding to the peak of activated macrophages in the alveolar spaces, but decrease after 28 days, probably caused by the progressive depletion of cellular reserves of the inhibitor. For this reason, it is acceptable that NINT may not have any effect upon it.

NINT treatment did not significantly reduce either the inflammatory infiltrate in the skin or lipoatrophy, which are the most evident changes induced by BLM administration through osmotic minipumps. This is in accordance with the evidence that, even though NINT has been approved for scleroderma, it has been shown not ameliorate the status of the skin [18,19].

Unfortunately, many pre-clinical readouts focused on evaluating antifibrotic treatments are terminal procedures which don't reflect the clinical situation. In this scenario, the inhibition of the drug group compared to vehicles remains the unique informative result, precluding any other intra-subject evaluation about the disease development.

Imaging technologies, such as micro-CT, allowed longitudinal studies in the same mice before (baseline) and after drug treatment as its own control [36].

This pre-clinical setting reflects a more relevant clinical situation along with a drastic reduction in both the variability and number of mice used.

The therapeutic protocol used for NINT, starting the treatment at day 14, could decrease the antifibrotic effect, as reported in the study, on different readouts; however, we are committed to bring out the real potentiality of the drug tested and no amplify the pharmacological activity.

NINT only partially reduced lung fibrosis progression in ILD patients [19], since it has been reported a decline in the forced vital capacity (FVC) despite the treatment of 52 weeks. In agreement with the clinical outcome, the progressive increase in poorly-aerated tissue observed in BLM and NINT groups, compare to baseline, revealed a worsening of lung fibrosis which was only partially reduced by the antifibrotic treatment.

Taking together, these findings light up the reliability of this model as a translational tool to profile new antifibrotic drugs.

In this study we pharmacologically validated a new murine model of ILD and SSc, using an FDA-approved antifibrotic drug.

We strongly believe that an integrative approach is needed in drug discovery to establish reliable, reproducible and robust readouts in order to better profile putative drug candidates. We sought to address the strengths and weaknesses of the relevant readouts, as well as the importance of their validation prior to use for drug discovery.

Declarations

Author contributions statement

FR, EF and FS: conception, design, and data collection. FR, EF, LR, MN, ZK, AG and FS: laboratory testing. FR, EF, LR, MN, ZK, AG and FS: data analysis and interpretation. FR, EF, LR, ZK, MN, GV and FS: drafting of manuscript. All authors contributed to the article and approved the submitted version.

Competing interests

The authors declare that this study received funding from Chiesi Farmaceutici S.p.A. The funder was not involved in the study design, data collection and analysis, decision to publish, or preparation of the manuscript.

GV, AG and FS are employees of Chiesi Farmaceutici S.p.A., that supported the research work. The remaining authors declare that the research was conducted in the absence of any commercial or financial relationships that could be construed as a potential conflict of interest.

Data availability

All datasets generated for this study are included in the article/Supplementary Information.

References

1. Giacomelli, R. *et al.* Interstitial lung disease in systemic sclerosis: current and future treatment. *Rheumatol. Int.* **37**, 853–863 (2017).
2. Asano, Y. & Varga, J. Rationally-based therapeutic disease modification in systemic sclerosis: Novel strategies. *Semin Cell Dev Biol* **101**, 146–160 (2020).
3. Meloni, F. *et al.* BAL cytokine profile in different interstitial lung diseases: a focus on systemic sclerosis. *Sarcoidosis Vasc Diffus. Lung Dis* **21**, 111–118 (2004).
4. Steen, V. D. & Medsger, T. A. Changes in causes of death in systemic sclerosis, 1972-2002. *Ann. Rheum. Dis.* **66**, 940–944 (2007).
5. Wijsenbeek, M. & Cottin, V. Spectrum of Fibrotic Lung Diseases. *N Engl J Med* **383**, 958–968 (2020).
6. Chua, F., Gauldie, J. & Laurent, G. J. Pulmonary fibrosis: Searching for model answers. *American Journal of Respiratory Cell and Molecular Biology* vol. 33 9–13 (2005).
7. Degryse, A. & Lawson, W. Progress toward improving animal models for idiopathic pulmonary fibrosis. *Am J Med Sci* **341**, 444–449 (2011).
8. Moore, B. B. *et al.* Animal models of fibrotic lung disease. *Am. J. Respir. Cell Mol. Biol.* **49**, 167–179 (2013).
9. Scotton, C. J. & Chambers, R. C. Bleomycin revisited: towards a more representative model of IPF? *Am. J. Physiol. Lung Cell. Mol. Physiol.* **299**, L439-41 (2010).

10. Mouratis, M. & Aidinis, V. Modeling pulmonary fibrosis with bleomycin. *Curr Opin Pulm Med* **17**, 355–361 (2011).
11. Perelas, A., Silver, R., Arrossi, A. & Highland, K. Systemic sclerosis-associated interstitial lung disease. *Lancet Respir Med* **8**, 304–320 (2020).
12. Harrison, J. & Lazo, J. High dose continuous infusion of bleomycin in mice: a new model for drug-induced pulmonary fibrosis. *J Pharmacol Exp Ther.* **243**, (1987).
13. Aono, Y. *et al.* Surfactant protein-D regulates effector cell function and fibrotic lung remodeling in response to bleomycin injury. *Am. J. Respir. Crit. Care Med.* **185**, 525–536 (2012).
14. Lee, R. *et al.* Bleomycin delivery by osmotic minipump: Similarity to human scleroderma interstitial lung disease. *Am J Physiol Lung Cell Mol Physiol* **306**, L736-748 (2014).
15. Ravanetti, F. *et al.* Modeling pulmonary fibrosis through bleomycin delivered by osmotic minipump: a new histomorphometric method of evaluation. *Am. J. Physiol. Cell. Mol. Physiol.* **318**, L376–L385 (2020).
16. Liang, M. *et al.* A modified murine model of systemic sclerosis: Bleomycin given by pump infusion induced skin and pulmonary inflammation and fibrosis. *Lab Invest* **95**, 342–350 (2015).
17. Watanabe, T. *et al.* Optimization of a murine and human tissue model to recapitulate dermal and pulmonary features of systemic sclerosis. *PLoS One* **12**, 1–14 (2017).
18. Kuwana, M. & Azuma, A. Nintedanib: New indication for systemic sclerosis-associated interstitial lung disease. *Mod. Rheumatol.* **30**, 225–231 (2020).
19. Distler, O. *et al.* Nintedanib for Systemic Sclerosis–Associated Interstitial Lung Disease. *N. Engl. J. Med.* **380**, 2518–2528 (2019).
20. Kolb, P. *et al.* The importance of interventional timing in the bleomycin model of pulmonary fibrosis. *Eur. Respir. J.* **55**, 1901105 (2020).
21. Jenkins, R. G. *et al.* An official American thoracic society workshop report: Use of animal models for the preclinical assessment of potential therapies for pulmonary fibrosis. *Am. J. Respir. Cell Mol. Biol.* **56**, 667–679 (2017).
22. Bayne, K. Revised Guide for the Care and Use of Laboratory Animals available. *Am. Physiol. Soc. Physiol.* **39**, 208–211 (1996).
23. du Sert, N. P. *et al.* The arrive guidelines 2.0: Updated guidelines for reporting animal research. *PLoS Biol.* **18**, 1–12 (2020).
24. Meganck, J. & Liu, B. Dosimetry in Micro-computed Tomography: a Review of the Measurement Methods, Impacts, and Characterization of the Quantum GX Imaging System. *Mol Imaging Biol* **19**, 499–511 (2017).
25. Gattinoni, L., Caironi, P., Pelosi, P. & Goodman, L. R. What has computed tomography taught us about the acute respiratory distress syndrome? *Am. J. Respir. Crit. Care Med.* **164**, 1701–1711 (2001).
26. Mecozzi, L. *et al.* In-vivo lung fibrosis staging in a bleomycin-mouse model: a new micro-CT guided densitometric approach. *Sci Rep* **10**, (2020).

27. Gallet, P. *et al.* Long-term alterations of cytokines and growth factors expression in irradiated tissues and relation with histological severity scoring. *PLoS One* **6**, 1–10 (2011).
28. Ruscitti, F. *et al.* Longitudinal assessment of bleomycin-induced lung fibrosis by Micro-CT correlates with histological evaluation in mice. *Multidiscip. Respir. Med.* **12**, 8 (2017).
29. Ravanetti, F. *et al.* Modeling pulmonary fibrosis through bleomycin delivered by osmotic minipump: a new histomorphometric method of evaluation. *Am J Physiol Cell Mol Physiol* **318**, L376-385 (2020).
30. Courtoy, G. E. *et al.* Digital image analysis of picrosirius red staining: A robust method for multi-organ fibrosis quantification and characterization. *Biomolecules* **10**, 1–23 (2020).
31. Wang, Y. *et al.* MBD2 serves as a viable target against pulmonary fibrosis by inhibiting macrophage M2 program. *Sci. Adv.* **19**, 1–13 (2020).
32. Brody, S. *et al.* Chemokine Receptor 2–targeted Molecular Imaging in Pulmonary Fibrosis. A Clinical Trial. *Am. J. Respir. Crit. Care Med.* **203**, (2020).
33. Huang, J. *et al.* Nintedanib inhibits macrophage activation and ameliorates vascular and fibrotic manifestations in the Fra2 mouse model of systemic sclerosis. *Ann. Rheum. Dis.* **76**, 1941 LP – 1948 (2017).
34. Bellamri, N. *et al.* Alteration of human macrophage phenotypes by the anti-fibrotic drug nintedanib. *Int. Immunopharmacol.* **72**, 112–123 (2019).
35. Oggionni, T. *et al.* Time course of matrix metalloproteases and tissue inhibitors in bleomycin-induced pulmonary fibrosis. *Eur. J. Histochem.* **50**, 317–325 (2006).
36. Ruscitti, F. *et al.* Longitudinal assessment of bleomycin-induced lung fibrosis by Micro-CT correlates with histological evaluation in mice. *Multidiscip Respir Med* **12**, (2017).

Figures

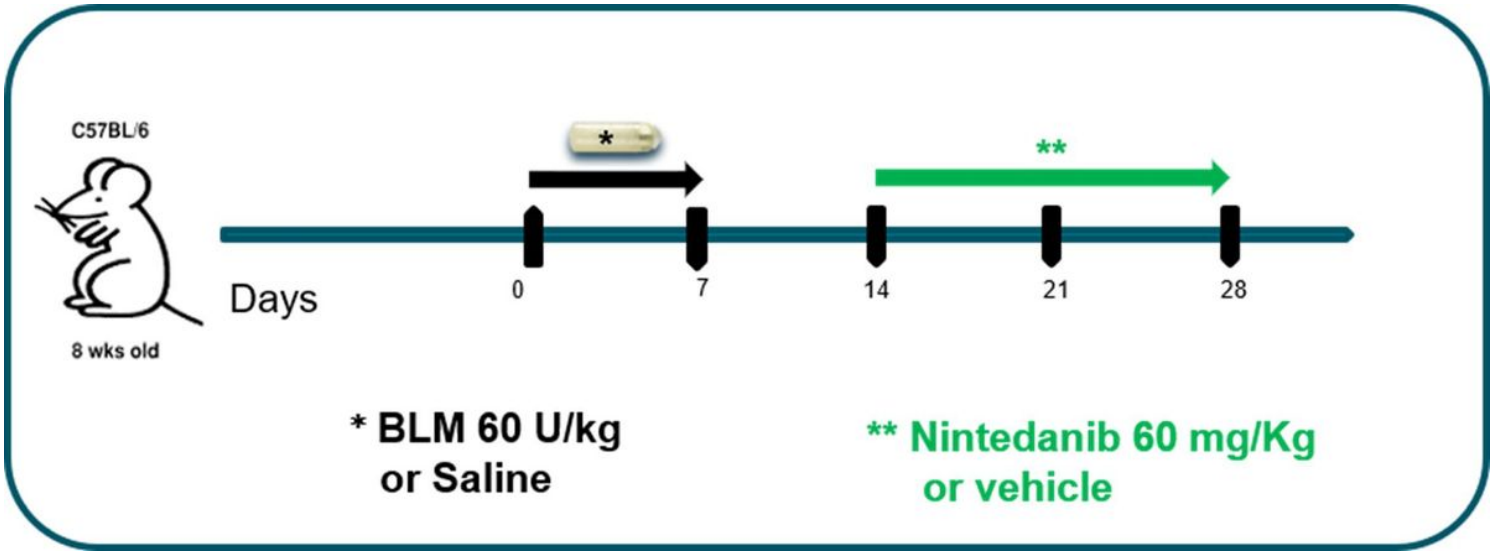

Figure 1

Experimental set up. Experimental timeline of bleomycin-induced lung mouse fibrosis by osmotic minipumps. 24 females C57BL/6 were randomly assigned to receive either saline (8 mice) or BLM (60U/kg) by osmotic minipumps at day 0. From day 14, 8 animals from BLM group received nintedanib and the others 8 received vehicle until day 28. At the endpoint, the effect of nintedanib was assessed by micro-CT and ex-vivo analyses.

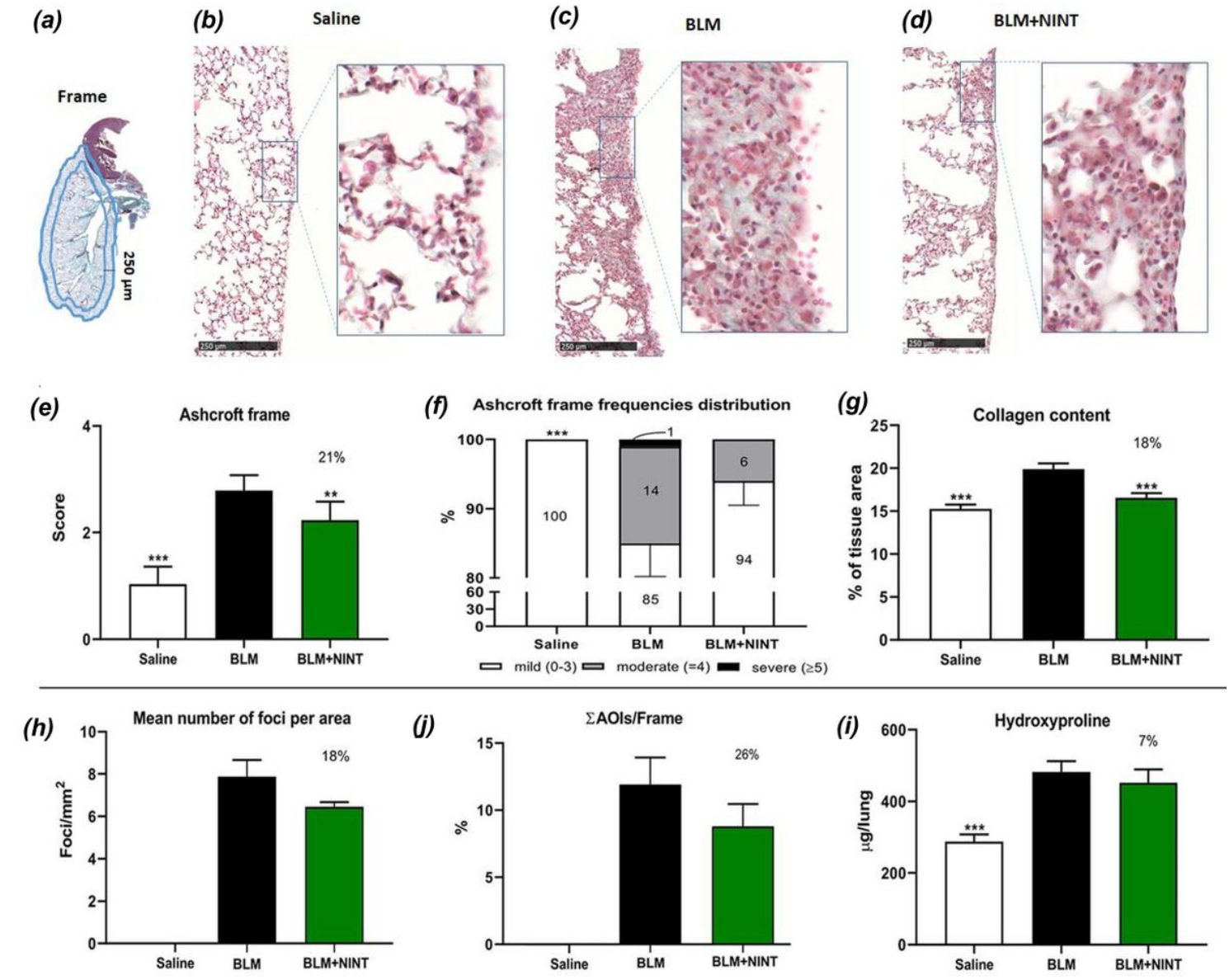

Figure 2

Histological and histomorphometric analysis of the subpleural parenchyma. Evaluation of the antifibrotic activity of nintedanib (on bleomycin induced lung fibrosis through osmotic minipumps) at day 28. A: Schematic representation of the Frame 250-µm thick considered as a region of interest. B-D: Representative microphotographs of the subpleural parenchyma of Saline (B), BLM (C) and BLM+NINT (D) treated groups at day 28 (MT staining; 10x magnification. The area within the rectangles has been magnified at 20x). E: Ashcroft score determination on the frame. F: Frequency distribution (%) of the Ashcroft scores values grouped as mild (0 –3), moderate (4) and severe (>5). G: Collagen content

determination expressed as a percentage of the tissue area. H: Mean number of fibrotic foci per mm2 of Frame. J: Global AOI area (AOIs) normalized on the Frame surface (AOIs/Frame) and expressed as percentage. I: Anti-fibrotic effect of NINT on hydroxyproline concentration in the right lung. Data are shown as mean ± S.E.M. for 8 mice per group. In D, F, G, H and I Saline and BLM+NINT were compared to the BLM group using one-way ANOVA followed by Dunnett's test (**P<0.01; ***P<0.001). In E statistical comparisons with the BLM group were performed using Chi-squared test (**P<0.01; ***P<0.001). The percentages on the BLM+NINT bars represent the inhibition effect of the treatment compared to BLM.

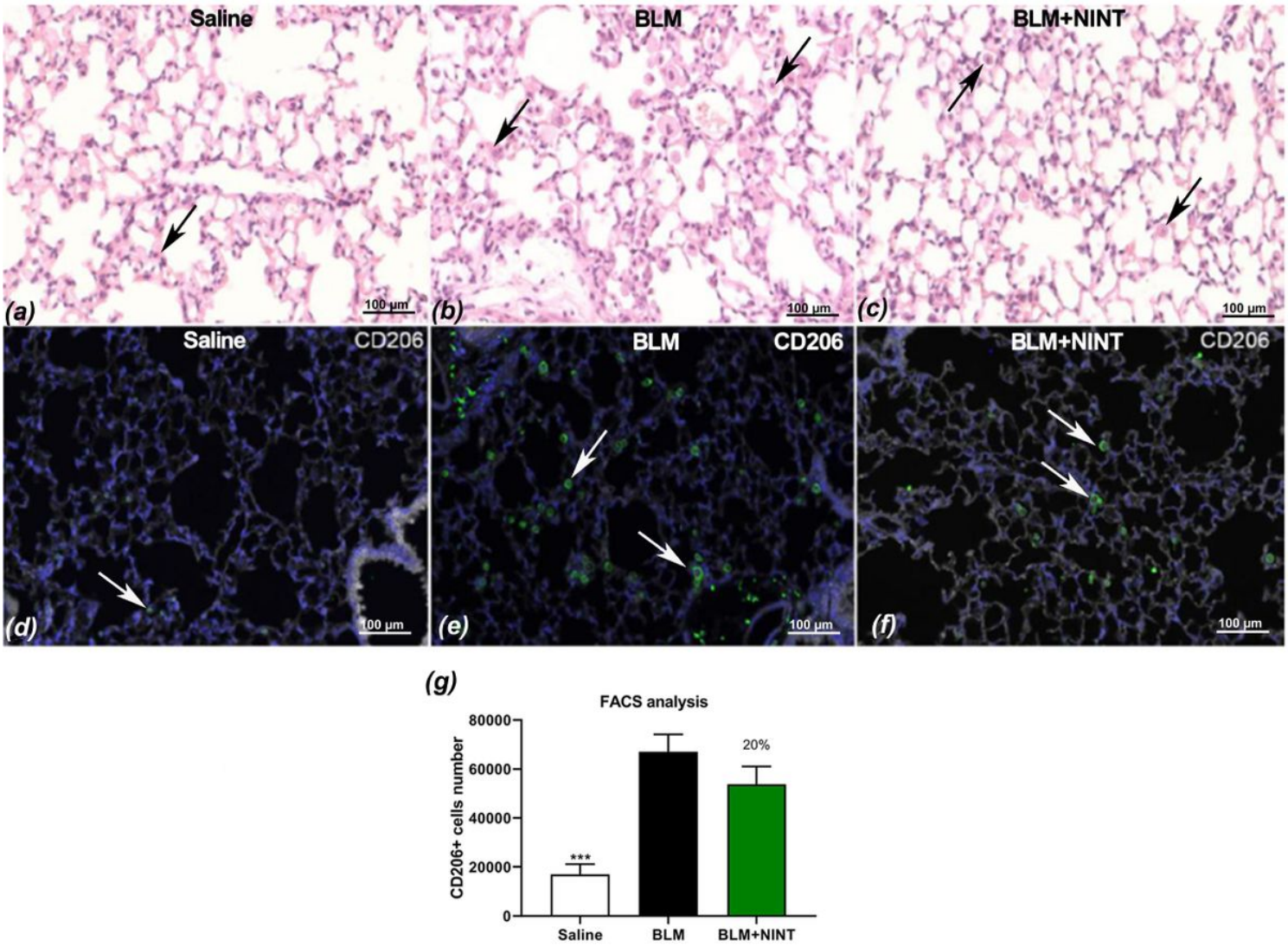

Figure 3

Detection of macrophages in the lung tissue and BALF. Representative microphotographs of sequential sections of lung tissue of saline (A and D), BLM, (B and E) and BLM+NINT treated mice (C and F) at day 28. (A, B, C: H&E staining; D, E, F: immunofluorescent staining for CD206 and DAPI). Residual macrophage cells in lung tissue after bronchoalveolar lavage are indicated with black arrowheads in the H&E images. White arrowheads indicate macrophages expressing CD206+ in IF images. G: Absolute number of CD206+ positive macrophages counted by FACS in saline, BLM and BLM+NINT-treated mice. Data are shown as mean values ± S.E.M. for 8 mice per group. Asterisks indicate significant statistical

differences in comparison with BLM group (***P<0.001; ANOVA followed by Dunnett's test). The percentage on the BLM+NINT bars represents the inhibition effect of the treatment compared to BLM.

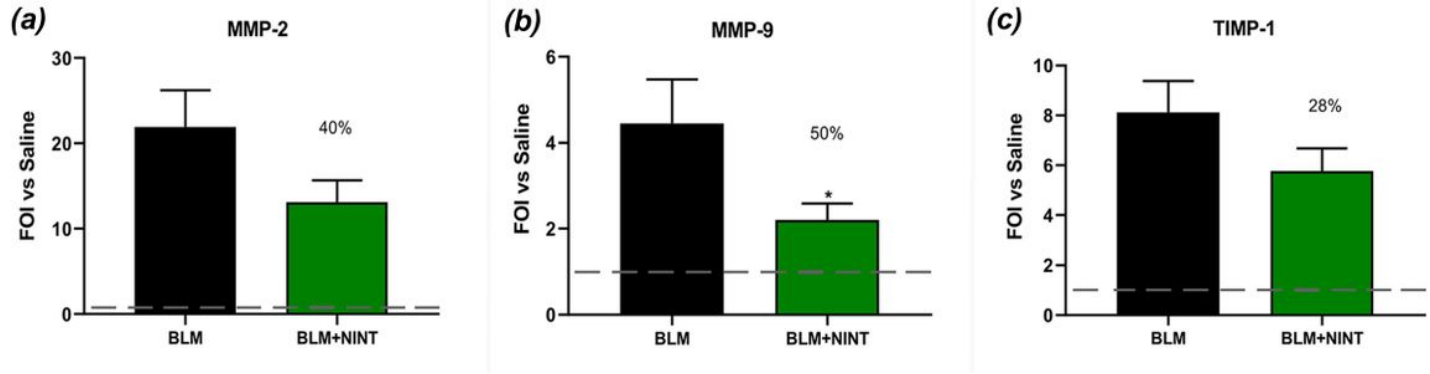

Figure 4

Evaluation of antifibrotic activity of nintedanib on matrix metalloproteinases at day 28 in BALF. MMP-2 (A), MMP-9 (B) and their inhibitor TIMP-1 (C) measured using the specific ELISA kit. The fold of increase vs Saline (FOI vs. Saline) for each group is shown as mean ± S.E.M. for 8 mice per group. The dashed lines indicate the saline values. Asterisks indicate statistical significance of each group vs. BLM (*P<0.05; one-way ANOVA followed by Dunnett's test). The percentages on the BLM+NINT bars represent the inhibition effect of the treatment compared to BLM.

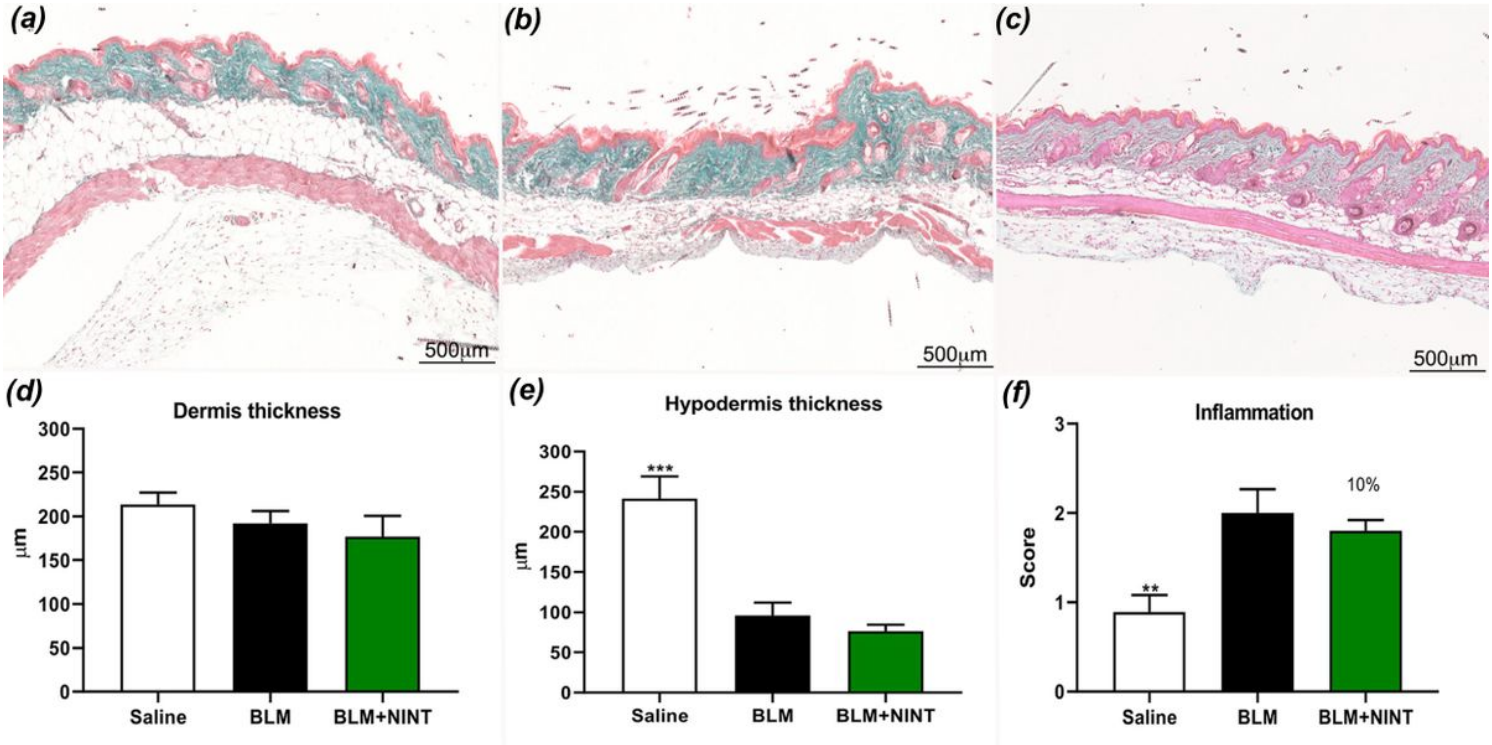

Figure 5

Histomorphometric analysis of dermal fibrosis. Evaluation of the antifibrotic activity of nintedanib on bleomycin-induced skin fibrosis through osmotic minipumps at day 28. Skin microphotographs of Saline (A), BLM (B) and BLM+NINT (C) treated animals (MT staining; 5X magnification). Measures of dermis

thickness (D), hypodermis thickness (E) and evaluation of the inflammation score (F) were carried out at five randomly selected fields from a sample of each animal. Data are shown as mean values ± S.E.M. for 8 mice per group. Changes were compared to the BLM group using one-way ANOVA followed by Dunnett's test (**P < 0.01; ***P<0.001). The percentages on the BLM+NINT bars represent the inhibition effect of the treatment compared to BLM.

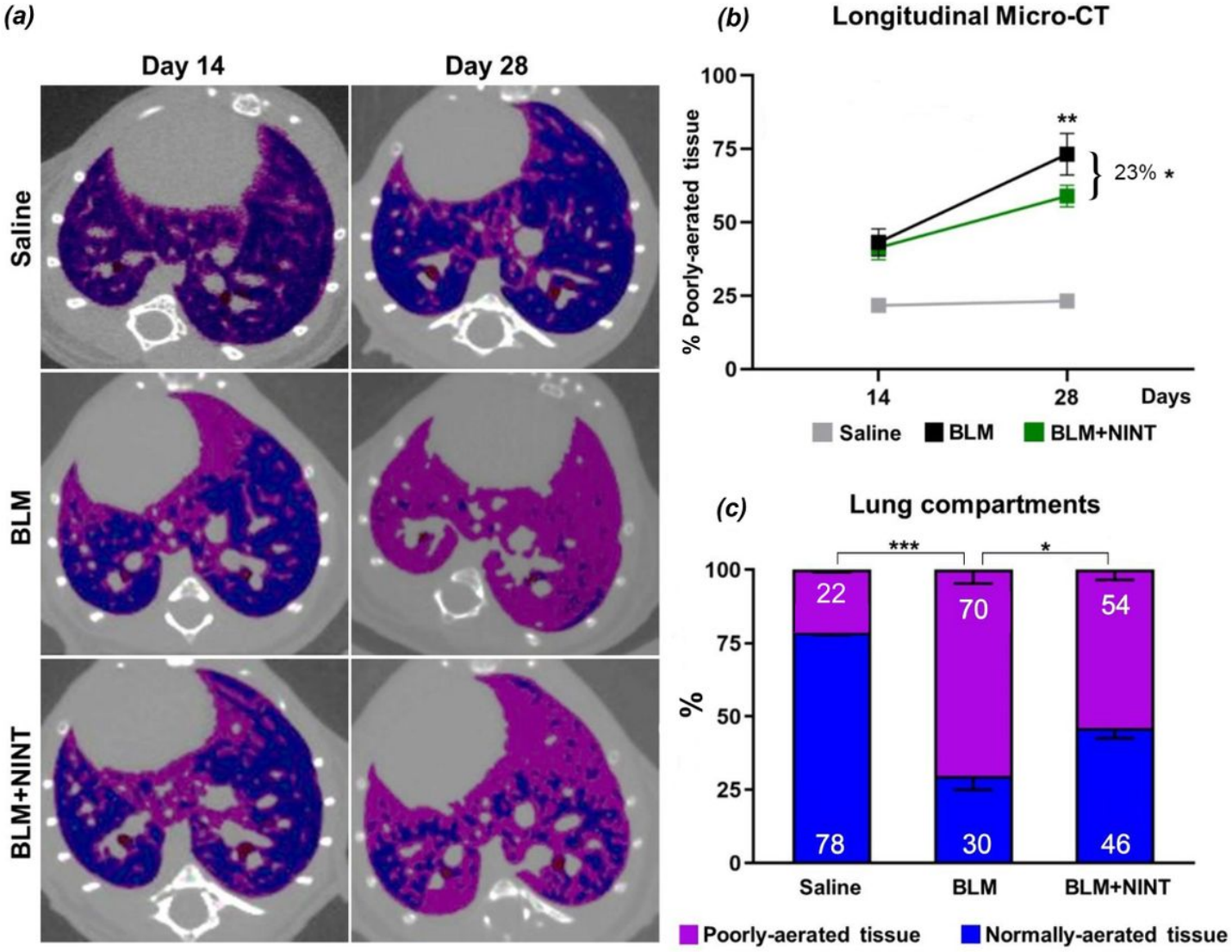

Figure 6

Longitudinal Micro-CT analysis. Representative Micro-CT images of Saline, BLM and BLM+NINT lungs divided in normally and poorly- aerated tissue (colored in blue and pink, respectively) at day 14 and 28 (A). Longitudinal Micro-CT quantification of poorly-aerated tissue at day 14 and 28 in Saline, BLM and BLM+NINT groups (B). Data are shown as mean percentages ± S.E.M. for 8 mice per group. Asterisks indicate statistical significance of each group at day 28 vs. day 14 (**P < 0.01; two-way ANOVA followed by Sidak's test). The inhibitory effect of NINT treatment has been calculated with respect to BLM group and reported at day 28 (*P<0.05; two-way ANOVA followed by Dunnett's test). Lung compartments quantification at day 28, the data represent the percentage of normally- and poorly-aerated tissue in

Saline, BLM and BLM+NINT-treated animals (C). Asterisks indicate statistical significance of each compartment in Saline and BLM+NINT vs. BLM (*P<0.05; ***P<0.001; Chi-squared test).

Supplementary Files

This is a list of supplementary files associated with this preprint. Click to download.

- SupplementaryFigures.pdf